Atmos. Chem. Phys. Discuss., 14, 12071–12120, 2014
www.atmos-chem-phys-discuss.net/14/12071/2014/
doi:10.5194/acpd-14-12071-2014

Atmospheric Chemistry and Physics Discussions

Microphysical properties of synoptic scale polar stratospheric clouds: in situ measurements of unexpectedly large HNO_3 containing particles in the Arctic vortex

S. Molleker[1], S. Borrmann[1,2], H. Schlager[3], B. Luo[4], W. Frey[1,*], M. Klingebiel[2], R. Weigel[2], M. Ebert[5], V. Mitev[6], R. Matthey[7], W. Woiwode[8], H. Oelhaf[8], A. Dörnbrack[3], G. Stratmann[3], J.-U. Grooß[9], G. Günther[9], B. Vogel[9], R. Müller[9], M. Krämer[9], J. Meyer[9], and F. Cairo[10]

[1]Max Planck Institute for Chemistry, Particle Chemistry Department, Mainz, Germany
[2]Institute for Physics of the Atmosphere, University of Mainz, Germany
[3]Deutsches Zentrum für Luft- und Raumfahrt (DLR), Institute of Atmospheric Physics, Oberpfaffenhofen, Germany
[4]Eidgenössische Technische Hochschule Zürich, Zürich, Switzerland
[5]Technical University Darmstadt, Darmstadt, Germany
[6]CSEM Centre Suisse d'Electronique et de Microtechnique SA, Neuchâtel, Switzerland

[7]Laboratoire Temps-Fréquence, Université de Neuchâtel, Switzerland
[8]Institute for Meteorology and Climate Research, Karlsruhe Institute of Technology, Karlsruhe, Germany
[9]Institut für Energie- und Klimaforschung (IEK-7), Forschungszentrum Jülich GmbH, Jülich, Germany
[10]Institute of Atmospheric Science and Climate, ISAC-CNR, Rome, Italy
[*]now at: School of Earth Sciences, The University of Melbourne, Melbourne, Victoria, Australia

Received: 6 April 2014 – Accepted: 14 April 2014 – Published: 13 May 2014

Correspondence to: S. Molleker (s.molleker@mpic.de)

Published by Copernicus Publications on behalf of the European Geosciences Union.

ACPD
14, 12071–12120, 2014

Abstract

In January 2010 and December 2011 synoptic scale PSC fields were probed during seven flights of the high altitude research aircraft M-55 *Geophysica* within the RECONCILE (Reconciliation of essential process parameters for an enhanced predictability of Arctic stratospheric ozone loss and its climate interaction.) and the ESSenCe (ESSenCe: ESA Sounder Campaign) projects. Particle size distributions in a diameter range between 0.46 µm and 40 µm were recorded simultaneously by up to four different optical in situ instruments. Three of these particle instruments are based on the detection of forward scattered light by single particles. The fourth instrument is a grey scale optical array imaging probe. Optical particle diameters of up to 35 µm were detected with particle number densities and total particle volumes exceeding previous Arctic measurements. Also, gas phase and particle bound NO_y were measured, as well as water vapor concentrations, and other variables. Two remote sensing particle instruments, the Miniature Aerosol Lidar (MAL) and the backscatter sonde (MAS, Multiwavelenght Aerosol Scatterometer) showed the synoptic scale of the encountered PSCs. The particle mode below 2 µm in size diameter has been identified as supercooled ternary solution droplets (STS). The PSC particles in the size range above 2 µm in diameter are considered to consist of nitric acid hydrates or ice, and the particles' high HNO_3 content was confirmed by the NO_y instrument. Assuming a particle composition of nitric acid trihydrate (NAT), the optically measured size distributions result in particle-phase HNO_3 mixing ratios exceeding available stratospheric values. In particular, with respect to the denitrification by sedimentation of large HNO_3-contaning particles, generally considered as NAT, our new measurements raise questions concerning composition, shape and nucleation pathways. Measurement uncertainties are discussed concerning probable overestimations of measured particle sizes and volumes. We hypothesize that either a strong asphericity or the particle composition (e.g. water-ice coated with NAT) could explain our observations.

ACPD

14, 12071–12120, 2014

1 Introduction

The main role of polar stratospheric clouds (PSC) for the stratospheric ozone related chemistry can be divided into two major processes. These are the heterogeneous chlorine activation (Solomon et al., 1986; Solomon, 1999) and the redistribution of water and nitric acid due to sedimentation of cloud particles leading to dehydration and denitrification, the latter of which slows down chlorine deactivation through the formation of $ClONO_2$ in the polar spring. Denitrification can extend the ozone depleting season in the late spring, depending on the persistence of the polar vortex, ultimately resulting in lower stratospheric ozone values (Waibel et al., 1999). In the last decades, different types of PSC particles have been studied (see overviews in Peter and Grooß, 2011; Peter, 1997) and the ongoing research still aims to quantify their contributions to polar ozone chemistry as well as the microphysical mechanisms underlying their formation. The most frequent type of PSC particles are liquid aerosols-supercooled binary (SBS) or ternary solution (STS) droplets consisting of sulfuric acid, water and, in the case of a ternary solution, additionally nitric acid. These liquid particles possibly dominate the chlorine activation (Wegner et al., 2012), which also still is a matter of scientific discussion. On the other hand, the major contribution to denitrification comes from solid nitric acid containing particles, which can grow to larger sizes leading to higher sedimentation speeds and efficient downward transport of nitrate compounds.

Solid nitric acid containing particles were suggested to exist in the form of hydrates (Crutzen and Arnold, 1986; Toon et al., 1986), although the nucleation processes of possible different hydrate types are not yet fully understood. Recent publications (Engel et al., 2013; Hoyle et al., 2013) show strong evidence for heterogeneous nucleation of solid PSC particles. A molar ratio of 3 : 1 of water to nitric acid obtained in balloon-borne measurements (Voigt et al., 2000) confirms the existence of most stable hydrate form – nitric acid trihydrate (NAT) – in the polar stratosphere. On the other hand, attempts to produce freely floating pure NAT particles in the lab failed so far, whereas nitric acid dihydrate (NAD) particles could be nucleated (Wagner et al., 2005, also in recent

ACPD
14, 12071–12120, 2014

AIDA[1] measurements), whereby the formation of metastable NAD is expected to be favored compared to NAT (Worsnop et al., 1993). Additionally, the nature of ice particles appears to be more complex as it also has been shown that a residual STS coating occurs during homogenous freezing of STS particles (Bogdan et al., 2010).

The particle measurements presented in this work were obtained mainly in the course of the RECONCILE field campaign in the winter 2009/2010 in Kiruna (67.8° N, 20.3° W). A comprehensive review of the RECONCILE campaign and the flight strategy of the Russian high altitude aircraft M-55 *Geophysica* are given in von Hobe et al. (2013). The first five of the 13 stratospheric flights occurred during the PSC season in the second half of January 2010. The minimum stratospheric temperatures in the polar vortex of the winter 2009/2010 were below the climatological mean (Dörnbrack et al., 2012) and low enough for formation of synoptic scale PSCs, as was widely observed by satellite lidar measurements (Pitts et al., 2011). The position of the polar vortex was shifted towards Europe (see Fig. 1) and moved over Sweden during the first part of the RECONCILE campaign. This aspect helped to accomplish long flight legs inside PSCs. Two additional flights with a reduced instrumentation were performed from the same location in Kiruna (Sweden) in December 2011 during the ESSenCe campaign (Kaufmann et al., 2013). In analogy to their Fig. 1 in Dörnbrack et al. (2012) for the temperature development in the Arctic stratosphere, a similar plot provides here context for the two flights in December 2011 (Fig. 2). This plot shows that probing of PSCs occurred about a week after a relatively early and strong temperature drop at the beginning of December. The development of the temperature in the vortex before and during the ESSenCe flights at the 30 hPa level is illustrated in Fig. 3 and the seven flight tracks with PSC encounters are displayed in Fig. 4.

As those cold synoptic conditions are relatively rare in the Arctic, previous in situ measurement have mostly documented mesoscale lee wave induced PSCs (Dye et al., 1992; Voigt et al., 2003; Lowe et al., 2006), only few presented PSC observations

[1]AIDA (Aerosol, Interactions, and Dynamics in the Atmosphere) cloud chamber

ACPD
14, 12071–12120, 2014

representative of synoptic conditions (Larsen et al., 2004; Weisser et al., 2006). The measurements of this study thus contribute to the investigation of PSC properties and particle formation on synoptic scales in the Arctic. One particular focus of our study is the occurrence of extraordinarily large PSC particles in high number densities. Here a closure problem arises as the total NO_y typically available within the polar vortex may not suffice to produce the corresponding large amounts of particle bound HNO_3.

2 Measurement techniques

Up to four different in situ optical particle instruments were deployed concurrently on the *Geophysica* aircraft. These were forward scattering spectrometer probes: FSSP-300 (Baumgardner et al., 1992, with the SPP-300 signal processing package upgrade from DMT Inc. Boulder, CO. USA), FSSP-100 (Dye and Baumgardner, 1984, also including an SPP) and the CDP (Cloud Droplet Probe, Lance et al., 2010, from DMT Inc.). The fourth instrument was a grey scale optical array probe with a 15 µm pixel resolution (CIPgs, Cloud Imaging Probe from DMT Inc., e.g. Korolev, 2007). The latter probe was initially considered as having a lower size detection limit not suitable for PSC detection, nevertheless this probe collected useful data in low level clouds as well as inside PSCs. These three instruments had been modified for the deployment under the ambient conditions at high altitudes as encountered by the M-55 *Geophysica*. Additionally the data of the condensation particle counter (COPAS, Curtius et al., 2005; Weigel et al., 2009, here of the COPAS channel counting particles with diameter larger than 15 nm) were used in the presented results. COPAS has a maximum detectable particle diameter of a few µm, a limit given by the aspiration efficiency of the aerosol inlet.

Due to electronic noise consisting of multiple counts triggered by real particles, several size channels of the FSSP-300 had to be discarded from the data, which resulted in a higher size detection limit of 0.46 µm. This corrected limit was found by the correlation analysis between the 5 lowest FSSP-300 size channels and by a comparison with

ACPD
14, 12071–12120, 2014

COPAS data, as the cloud particle number density reported by the FSSP-300 should not exceed the total aerosol number density detected by COPAS.

2.1 Detection limits and sizing

The comparison of the measurements of the two FSSPs of different lower size limits helped to understand the discrepancy of 1–2 orders of magnitude in the overlapping size bin between 1 and 2 µm (Fig. 5). In this region, a steep slope in the particle size distribution coincides with the ambiguity of the Mie calibration curve and a decreasing sensitivity of the FSSP-100. As a consequence, the lower detection limit of the FSSP-100 was corrected from 0.8 to 1.05 µm.

The lower limit in particle detection of the CDP would be at a diameter of about 3 µm. However, due to instrumental problems related to extremely low ambient temperatures and insufficient heating during the CDP's first deployment in the stratosphere only in the last PSC-flight of the RECONCILE campaign particles larger than 7 µm were detected with the size distribution shown in Fig. 6. In the two ESSenCe flights two years later additional measures had been taken, and the CDP performed well. The upper size diameter limits of both FSSP instruments and of the CDP instrument were at 37 to 50 µm.

The sizing accuracy of the scattering probes (i.e. FSSP-100, FSSP-300, and CDP) is estimated to be about 10 % for spherical objects and correctly assumed refractive indices of the particles. However, the uncertainty is much higher in the regions with ambiguities in the Mie curve on which the sizing calibration is based. The bin limits of the FSSP probes were defined with the intention to fully contain ambiguities of the Mie curve, especially in the lower size range (i.e. 0.46–5 µm), to avoid falsified size classifications. The sizing calibration was calculated for the refractive index of NAT, with $n = 1.48$ taken as an average from the publications of Middlebrook et al. (1994) and Toon et al. (1990). The refractive index of STS ($n = 1.42$, depends on composition) is given in Krieger et al. (2000) and Luo et al. (1996). The Mie curve for STS in the relevant size range below 1 µm is within 10 % of size accuracy close to the Mie curve of

ACPD
14, 12071–12120, 2014

NAT. The resulting size binning tables for the FSSPs are updated and adapted versions of those by Dye et al. (1992) and Borrmann et al. (2000a).

2.2 Sample areas, number densities and counting statistics

The instruments' sample volumes for particle number density measurements were calculated as a product of the true air speed (from aircraft data) multiplied with the instrument-specific effective detection area, which is the so-called sample area. Values for the sample areas of the three forward scattering probes were measured by means of a newly designed calibration device in our laboratory similar to the one described by Lance et al. (2010). This was done before and after each campaign by scanning the instrument sample areas with a monodisperse droplet stream originating from a piezoelectric droplet generator. The following sample area values were used for the analysis of the PSC data: 0.09 mm^2 for FSSP-300, 0.42 mm^2 for FSSP-100, and 0.22 mm^2 for CDP. The respective uncertainties of these values are 10 % for CDP and 15 % for FSSPs.

With regard to the given sample areas one has to keep in mind that typical particle concentrations of PSCs result in very low counting statistics. While the STS mode and background aerosol was present with concentrations in the range of 1–10 cm^{-3} (resolved only with FSSP-300), the concentrations of particles with diameters above 1–2 µm lie in the range below of 10^{-2} cm^{-3} decreasing further for larger particles to below 10^{-3} cm^{-3} at diameters above 10 µm. The encounters of the FSSP-100 within long flight legs inside PSCs average to about 1 particle within 4 s corresponding to a flight distance of about 0.75 km between single detections. Consequently, time series for particle diameters above 2 µm were averaged over 100 to 200 s. Averaging times of 500 s were used in the case of particle volume calculations where relatively large but rare particles contribute significantly. The counting statistics for the FSSP-300 are even lower, since its sample area is about a factor of 5 smaller than that of the FSSP-100. The more confined detection range of the CDP was above 7 µm and its relatively high ratio of Depth of Field (DoF) rejected to accepted particles could be used to validate

ACPD
14, 12071–12120, 2014

the FSSP-100 measurements by deriving the concentration from the CDP time series records of DoF rejected particles. This can be done because events of DoF rejection can be viewed as real particles, the presence of which was detected albeit without sizing. The result for a ratio of 20 for rejected to accepted particles is illustrated in the Fig. 7b, where the corresponding FSSP-100 concentration for diameters above 4.7 µm is in a very good agreement with the CDPs DoF rejected counts of much lower statistical uncertainty. Since the number counts for DoF rejection depend on particle size, the used rejected to accepted ratio was looked up from cloud measurements (at low levels in the Arctic) of narrow quasi-monomodal size distributions for particle diameters in the considered range between 12 and 16 µm.

Since our FSSP-300 has undergone several modifications (e.g. of hardware, optics, control software and alignments) between its first deployment in the Arctic lower stratosphere on M-55 *Geophysica* in 1996 (Borrmann et al., 2000b) and 2010, specific time periods of both data sets were selected. These cover periods with comparable background aerosols inside of the polar vortices, which represent particles with sizes at the FSSP-300's lower detection limit. For these smallest particles the instrument is most susceptible with respect to alignment errors and electronic noise problems. The corresponding comparison of size distributions is shown in (Fig. 8). With the given uncertainty in counting statistics the background aerosol size distributions agree quite well and we conclude that the instrument's main characteristics have not changed throughout all the implemented modifications.

2.3 Inter arrival time analyses

The particle by particle (PbP) data capability of the CDP allows a so-called inter arrival times analysis. Figure 9 shows an example of the CDP measured distribution of inter arrival times (IAT) of PSC particles during the flight on 11 December 2011 suggesting a relatively homogeneous and random distribution of large PSC particles over a "spaghetti" of 0.22 mm^2 cross section and 400 km length. Such analyses are usually less confident with these instruments in the much smaller lee-wave PSCs. The homo-

ACPD
14, 12071–12120, 2014

geneity statement refers to scales larger than a mean average distance of about 1 km between particle detections. Nevertheless, this distribution does not show significant variations in the number density, which would be expected in a lee wave induced PSC field. Based on such distributions measurement artifacts like shattering or electronic noise could have been identified by increased numbers of short particle inter arrival times. Unlike for other measurements in cirrus (e.g., de Reus et al., 2009; Frey et al., 2011) such effects were not found in the PSC data. Although FSSPs lacked the PbP data record, the low numbers of counts per second in PSCs made a similar, but coarser analysis possible. The fraction of one second (i.e. instrument's integration interval) values with more than one count agreed to the estimated low probability for an average count rate of one particle in a few seconds based on Poisson statistics. Consequently, artifacts were not found in the data. Also, shattering usually is associated with much larger particle sizes (i.e. > 100 µm in diameter) for these instrument geometries.

2.4 The optical array probe and further instrumentation

Cloud Imaging Probe: although optical array probes are designed mainly for measuring sizes and shapes of ice crystals larger than roughly 50 to 100 µm, the CIP grey scale collected data in PSCs just at the lowermost limit of its particle size resolution. The total numbers of large ($D > 20$ µm) solid PSC particles detected by the scattering probes correlates from flight to flight with the number of 2 to 6 pixels events detected by the CIP grey scale in the same PSC fields (Fig. 10). At maximum 149 such images were detected in one flight (25 January 2010) over a flight distance of 1200 km.

Reactive Nitrogen (NO_y) instrument: the optical particle measurements were juxtaposed with data from the NO_y instrument SIOUX (Voigt et al., 2005), which was sampling with one forward and one rear facing inlet measuring total and gas phase NO_y, respectively. The total NO_y signal was capable of resolving individual HNO_3 containing particles with sizes greater than 5 µm and ambient number densities smaller than $0.0004\,cm^{-3}$ as single peaks in the 1 Hz signal data time series. Here, we use only the detected individual NO_y containing particles which were analyzed according to the

ACPD
14, 12071–12120, 2014

single particle detection method as described by Northway et al. (2002). Details of the entire NO_y data set will be presented in a separate paper.

Aerosol Backscatter sonde: the bulk optical properties of the particle population were detected by the aerosol backscatter sonde MAS (Cairo et al., 2004). The instrument is basically a near range lidar that probes the atmosphere from 3 to 150 m from the aircraft. It fires a 532 nm, 1 ns laser pulse and detects the light return from air molecules and aerosol particles resolved in two polarization channels. The instrument thus delivers aerosol volume backscatter coefficients and depolarization profiles with a time resolution of 5 s and a spatial resolution of 25 cm perpendicular to the aircraft's flight path. In the present work we report aerosol depolarization values computed for aerosol backscatter ratio (ratio of aerosol to molecular volume backscatter coefficients) greater than 1, as above that value we can provide absolute uncertainties below 5 %.

Miniature Airborne Lidar (MAL): the range-resolved backscatter and depolarization profiles are obtained with two independently operating standalone lidar instruments installed on the aircraft, referred to respectively as MAL1 (probing in upward direction) and MAL2 (probing in downward direction) Mitev et al. (2002). The lidars use a Nd : YAG micropulsed laser at a wavelength of 532 nm. The altitude- and time-resolution of the signal acquisition is about 20 m and 6 s, respectively; but in the data processing the resolutions are degraded, in order to achieve adequate signal-to-noise ratio. An intercomparison of the total backscatter and depolarization backscatter coefficients measured by the two MALs and CALIPSO-CALIOP lidar (Pitts et al., 2011) was also performed during RECONCILE campaign (Mitev et al., 2012).

Water Vapor: a Hygrometer based on Lyman-alpha fluorescence technique (FISH, Fast In situ Stratospheric Hygrometer, (Zöger et al., 1999)) was deployed on the aircraft. Here water vapor mixing ratios are used for the calculation of the frost point and the equilibrium temperature of NAT.

Air temperature: the ambient temperature measurements with an accuracy of 0.5 K (only RECONCILE) were provided by the instrument called TDC (Thermo Dynamic

ACPD
14, 12071–12120, 2014

Complex (Shur et al., 2007)). During ESSenCe a different temperature instrument (aircraft data) had to be adopted with higher uncertainty of +0.5/−1.5 K.

MIPAS-STR: Volume mixing ratios of various trace gas species, temperature and cloud parameters were derived from the MIPAS-STR (Michelson Interferometer for Passive Atmospheric Sounding – STRatospheric aircraft) passive infrared limb observations (Woiwode et al., 2012, and references therein). Here HNO_3 profiles obtained during the RECONCILE season are used for comparison with the in situ data.

3 Observations and results

In total, about 13 flight hours over 7 flights were spent inside PSCs. Continuous PSC fields in flight legs of more than one hour corresponding to about 700–900 km illustrate the synoptic scale character of PSCs in both winters. Figure 11 shows a MAL profile with a flight leg inside a 900 km long PSC field of the flight on 20 January 2010. Time series of three flights (Fig. 7) show number concentrations mostly derived from FSSP measurements together with temperatures relevant for PSC existence. For the calculation of the NAT equilibrium temperature T_{NAT} (Hanson and Mauersberger, 1988) water vapor concentration measurements of the FISH instrument and NO_y data of the SIOUX instrument were used. In the absence of NO_y data, the values of 5 and 10 ppbv were used as upper and lower estimates. For the calculation of the frost point the parameterization of Marti and Mauersberger (1993) and the FISH data were applied. Most of the PSC measurements were obtained at the flight altitude of about 18 km, with a maximum altitude just below 19 km and lowest altitudes inside PSCs at 16.8 km. Thus, our investigations are limited to the lower altitude levels of PSC occurrence.

The number density measured by the FSSP-300 shows an anti-correlation with temperature and reaches the values measured by COPAS at the lowest temperatures around 188 K. For events like these it can be assumed that the background aerosol was almost completely activated to cloud elements, which implies that the STS-mode particles grow to sizes above the FSSP's lower detection threshold. The COPAS count

ACPD
14, 12071–12120, 2014

levels were in the 6–14 particles cm^{-3} range and thus the COPAS instrument provides an upper limit for the maximum concentration possibly detected by the FSSP-300. The FSSP-300s total number density did not exceed COPAS values, as evident from Fig. 7a.

3.1 Ternary solution droplet mode

The collected FSSP size distributions show two distinct particle modes. In most of the measured size distributions the particle number density spans 2–3 orders of magnitude over a size diameter range from 1 to 2 µm, which also can be seen from the time series of different sizes in Fig. 7a. Additionally, in some time intervals the particle concentration in the size interval from 2 to 5 µm is lower than in the size range above, indicating a separation of the two particle modes. Clearly, owing to fast sedimentation (about 1.7 cm s^{-1} for a 14 µm large NAT particle), the particles from the upper and lower size modes originate from different air masses.

The interpretation of the sub-micron particle mode, which was partly resolved by the FSSP-300 measurement as the STS-mode, can be tested by its particle volume vs. temperature dependence. The dependence of particle volume on ambient temperature in PSCs consisting of STS is driven by the increased uptake of water and HNO_3 with decreasing temperature. The particulate volumes were calculated from the measured number size distributions and the particle volume plotted as a function of temperature (as discussed in Peter, 1997). Also included are STS-mode volumes derived from theory based on STS thermodynamics following Carslaw et al. (1995). The theoretical volumes of the STS particle mode shown as solid black lines in Fig. 12 were calculated accounting for the FSSP-300's detection limit – in our study at 0.46 µm –, which differs from the limits of this instrument in Dye et al. (1992), and Peter (1997). Four theoretical curves representing STS with different values for assumed HNO_3 mixing ratios of 2, 5, 10 and 15 ppbv are shown. With the intent to exclude the NAT phase the particle volumes were evaluated from the FSSP-300 size distributions only including diame-

ACPD
14, 12071–12120, 2014

ters less than 2 µm (points marked as crosses) while particles with larger sizes (also present in the same size distributions) were excluded from the volume determination. The STS particulate volumes calculated this way show a reasonably good agreement with the theoretical particle volume dependence of STS. The time intervals considered here were selected from parts of the flight track with a wider temperature range, which for given flight profiles implied that the aircraft did not stay on a constant potential temperature altitude level (altitude range of up to 1.5 km). Therefore, the airmass content of – in particular – HNO_3 is not expected to be constant. Also the calculation of volume curves for STS does not account for possible partitioning of HNO_3 into larger solid particles (e.g. NAT) which were always present in these measurements.

The finding that STS particles were present in large number densities is corroborated by the lidar measurements shown in Fig. 13 where a scatterplot of aerosol depolarization vs. backscatter ratio is reported. Here the long-range lidar MAL (red crosses) and the near-range backscatter sonde MAS probed the same 20 January PSC (black crosses) as shown in Fig. 11. Also PSC data from 17 January (green squares) and 25 January (blue squares) are included in Fig. 13. While the latter show depolarization around 9 %, indicating a detectable presence of solid particles, the former two displayed no significant aerosol depolarization, confirming that the STS particle contribution to the optical characteristic of these clouds was dominant. Nevertheless, some signal in the depolarization channel is still present and indicates that solid particles, probably NAT, with number densities much below those of the STS droplets, always were present embedded in the predominant STS clouds. The temperature dependence of the STS-Mode corresponds well to the strong anti-correlation of the FSSP-300 number concentration with temperature. The time series of the number concentration from the FSSP-300 in Fig. 7a can be interpreted as the varying fraction of the STS-mode above the instrument's detection limit of 0.46 µm. At the lower temperatures of about 187 K the FSSP-300 measured almost the same particle number density as the COPAS instrument in the channel for particles larger 15 nm. At slightly warmer temperatures the STS droplets right at the lower detection limit of the FSSP-300 may be just about too

ACPD
14, 12071–12120, 2014

small to be detected by the instrument. Thus with changing temperature STS droplets smaller than 0.46 µm may "grow into or shrink out of" the detection limit of the FSSP-300. This behavior also is illustrated for size distributions measured in air of different ambient temperatures (Fig. 14), where the difference is discernible in the FSSP-300 data and in the first one to two bins (e.g. below 1.9 to 3.3 µm) of the FSSP-100 data.

3.2 NAT and large particle mode

Throughout all PSC-flights the particles above 2 to 3 µm in diameter were frequently present in number concentrations of up to 0.8×10^{-2} cm^{-3} (Fig. 7c). Considering that the in situ recorded ambient temperatures mostly were 2–5 K above the frost point but still below T_{NAT}, the assumption that these larger particles consist of NAT seems plausible (Dye et al., 1992). The volume of the particle phase evaluated for diameters above 2 µm also is included within the volume vs. temperature graph of Fig. 12 as filled symbols. Many of these data points for volume fall into an area near the schematically drawn dashed line for NAT. These data points were calculated using 500 s flight time intervals to reduce errors due to counting statistics. Furthermore, it can be seen from the figure that some data points of the ESSenCe measurements were recorded above the NAT equilibrium temperature (T_{NAT}), and hence the particles were in a non-equilibrium state, which means here they were evaporating. On the other hand, ambient temperature was measured with higher uncertainty during ESSenCe flights (+0.5/−1.5 K) compared to the accuracy of the TDC used throughout RECONCILE. Therefore, a data point with 2 K above T_{NAT} might be partly attributed to a positive bias in the temperature measurement.

Maximum values of particle volume, arising from the part of the particle size distribution with diameters above 2 µm, correspond to distributions with shapes as those depicted in Figs. 14–15. It is worthwhile noting that these distributions represent particle volumes slightly (as in left panel of Fig. 15) or significantly (as in right panel of Fig. 15 for the 11 December 2011 ESSenCe flight) bigger than what was reported from other Arctic measurements (e.g., Brooks et al., 2003; Fahey et al., 2001). As instance,

ACPD
14, 12071–12120, 2014

during the ESSenCE flight we observed particle volumes which are twice as big as previously reported. The main contribution to the particle volume results from particles with diameters close to the mode maximum at 12 to 15 µm (e.g. Fig. 15). Unfortunately, the NO_y instrument was not deployed during the ESSenCE flights.

Evidence that these large particles contain HNO_3 is provided by the NO_y-instrument SIOUX which detected a high amount of HNO_3 in the particle phase, whereby no instrumentation to measure the molar ratio with respect to water in the particles was available. Partly due to a large enhancement factors F for particles with diameters above 10 µm (with F roughly between 10 to 18) and the relatively high overall particle number density the total NO_y signal of the instrument went into saturation in time intervals when most noticeable size distributions were obtained. Examples for this are shown in Figs. 6 and 14 (right panel). For two time intervals with particle concentrations below 0.002 cm^{-3} and where the NO_y instrument was not saturated two size distributions have been retrieved from the NO_y data by the single particle detection method as described by Northway et al. (2002) (Fig. 16). Particles sizes were calculated assuming spherical shapes and a NAT composition. The sensitivity of the method scales with particle volume, resulting in a lower detection size diameter limit of 5 µm. The discrepancy between the values obtained with NO_y and optical particle detection seems to repeat the findings of Brooks et al. (2003) (optical) and Fahey et al. (2001) (NO_y), where the optically detected particle number densities exceeded those obtained from the NO_y signal as well. Additionally, such discrepancies are compatible with the assumption of aspherical particle shapes, because in these cases the real enhancement factor of the inlet would be lower, especially for smaller particles.

Despite such uncertainties in the number density and the discrepancy with the optically measured size distribution, the NO_y retrieval provides trustworthy volume equivalent sizes for the assumed NAT composition of up to 20–24 µm particle diameter – keeping in mind that only unsaturated time intervals were evaluated. The uncertainty of the individual particle size calculation assuming NAT is estimated to 20 %. Additional support for the presence of large PSC particles comes from the CIPgs image

ACPD
14, 12071–12120, 2014

data (Fig. 10). The numbers of images recorded by the CIPgs are shown in the Table 1, where these numbers are compared to numbers of FSSP-detections above two particle diameter thresholds, 15 and 20 µm. The particle numbers revealed from two independent instruments and different measurement techniques seems to correlate. The estimated sample area of the CIPgs instrument for a 15 µm particle diameter is about 0.5 mm^2, which is slightly larger but close to that of the FSSP-100 with its value of 0.42 mm^2. We consider these triggered pixels as first quasi-visual evidence for the existence of large NAT rock type particles.

During the RECONCILE and ESSenCe flights within the polar vortex also impactor sampling of particles in the size range 100 nm–10 µm was applied. Within 11 RECONCILE flight-samples a variety of large non-volatile particles (of size diameters from 500 nm to 5 µm) could be collected for a posteriori analyses in the laboratory. In (Ebert et al., 2014) analyses are provided of the size, chemical composition and the morphology of individual particles within these samples by scanning electron microscopy.

The 759 analyzed non-volatile particles were found to be around 30 % silicates, 20 % Iron rich and 6 % carbon/silicate mixtures. Many of these particles will have extraterrestrial origin. But further on, around 10 % Ca-rich particles were found, which were recently also described by Corte et al. (2013) and 30 % of the particles show a composition which is similar to certain anthropogenic metal alloys (variable composition of Al, Cr, Mn, Fe, Ni, Cu, Zn). In the NASA cosmic dust catalog (Warren et al., 2011) such "alloy-like" stratospheric particles are partly classified as cosmic and partly as artificial terrestrial contamination.

In contrast to this finding these large non-volatile particles were almost completely absent in all RECONCILE and ESSenCe samples, which were taken within distinct PSC events. Inside the PSC only a little number (116) of small (< 500 nm) non-volatile particles could be found. Besides around 35 % Mg-rich silicates and 25 % Fe-rich particles, most likely of meteoric origin, also 25 % aluminum oxide spheres possibly from rocket launches were detected, as well as 15 % lead-rich particles from an unknown source.

ACPD
14, 12071–12120, 2014

4 Discussion and open questions

By assuming a NAT composition, the FSSP particle measurement can be expressed in terms of HNO_3 mixing ratio in the condensed phase. Such HNO_3 mixing ratios (particle phase only) were calculated using particle data averaged over 500 s and resulted in maximum values of up to 17 ppbv (January 2010) and up to 25–35 ppbv (11 December 2011). To put these numbers into perspective some of the particle plus gas phase HNO_3 mixing ratios were included in Fig. 17, which shows HNO_3-profiles obtained by the infrared limb-sounder MIPAS-STR deployed on the same aircraft (the vertical resolution of the shown retrieval results is about 1 km). A maximum re-nitrification magnitude of about 9 ppbv (from 7 to 16 ppbv) peaking around 405 K potential temperature is found by the end of the RECONCILE PSC season at the end of January 2010 (Woiwode et al. (2014); Fig. 2).

At this point it is uncertain, how much overestimation of particle-derived HNO_3 can be explained by a large spatial averaging of the remote sensing instrument, although the particle data have been averaged over long spatial intervals too (about 90 km). Different air volumes are observed by MIPAS-STR and the in situ instruments because the MIPAS-STR limb observations integrate radiation along the viewing direction approximately perpendicular to the flight track, with the largest contributions arising from the region around the tangent points of the observations. These are between a few tens to few hundreds of kilometers away from the flight path of the *Geophysica* depending on the tangent altitude. The in situ gas-NO_y measurement showed maximum values of 10 to 14 ppbv HNO_3 at the potential temperature levels corresponding to the renitrified layer (24–25 January). The Chemical Transport Model CLaMS provides maximum values of 16–17 ppbv for the total HNO_3 (Grooß et al., 2014). Contrary to that, the particle volume detected on 11 December 2011 corresponds to mixing ratios of 25–35 ppbv of HNO_3, and questions concerning the assumptions arise, as such values exceed any measured HNO_3 mixing ratio in the Arctic stratosphere.

ACPD
14, 12071–12120, 2014

Besides the high particle volume or HNO_3 content, NAT particle sizes above 10 µm in diameter are increasingly constrained by growth time and related sedimentation times and altitudes. A backward model calculation starting from the PSC field of the flight track on 11 December 2011 can accommodate a NAT particle of only up to 16 µm, where already by 20 % increased growth rate and by 10 % reduced sedimentation speed were assumed in the model (LAGRANTO trajectories based on ERA-Interim data). Similar results in Fahey et al. (2001) showed that only particles of up to 16–18 µm in diameter (so called "NAT-Rocks") exhibit realistic back trajectories, whereby these particles needed up to 4 to 6 days to grow to such sizes. Contrary to such theoretical considerations our FSSP size distributions from inside synoptic scale PSCs extend to optical particle diameters of up to 35 µm (Figs. 6 and 15), although just very few particles of diameters larger than 24 µm were recorded.

In Fig. 15 also simulated size distributions are shown. These were created by the Chemical Lagrangian Model of the Stratosphere (CLaMS) that includes a Lagrangian NAT particle scheme (Grooß et al., 2014; Kaufmann et al., 2014). The NAT particles were nucleated using a saturation-dependent nucleation scheme (Hoyle et al., 2013). Particle growth, evaporation and sedimentation were simulated along trajectories for the individual so-called particle parcels. For the comparison with the observations, all particle parcels within 100 km of the chosen flight path segment were taken into account. As also can be seen for another flight on 22 January 2010 (Grooß et al., 2014) the simulated NAT size distribution peaks in the same order of magnitude as do the observations, although NAT particles with diameters larger than 10 um are not reproduced by the model.

The FSSP-derived diameters for spherical particles combined with an assumption of a pure NAT composition seem to overestimate HNO_3 content in the condensed phase. Moreover, microphysical model simulations coupled to computed sedimentation speeds fail to reproduce the largest observed particles. Two hypotheses or a combination of both can help resolving such discrepancies: (a) strong asphericity of NAT particles, affecting both sedimentation and optical sizing and (b) an additional particle

ACPD
14, 12071–12120, 2014

type consisting of a NAT layers on ice-particles, as suggested earlier by Peter et al. (1994).

4.1 Hypothesis 1: aspherical large NAT particles

There is still a lack of direct measurements of the morphology of large HNO_3-containing PSC particles since most laboratory experiments for example concerning their heterogeneous chemical reactivity had been carried out with NAT deposits on substrates. Thus, it can only be speculated about the precise particle shapes. In Woiwode et al. (2014) different particle shapes with implications for sedimentation speeds are discussed and used to model the redistribution of HNO_3 which is then compared to measured vertical HNO_3 profiles. The comparison favored sedimentation speeds reduced by about a factor of 0.7.

It is clear that the degree of asphericity affects the size calibration of the FSSP. In Borrmann et al. (2000a) moderate asphericities of up to 1 : 2 were tested for the FSSP configuration using the T-matrix method. The results stated that the scattering cross section averaged over all orientation is still close to the Mie calculation. On the other hand, the asphericity would broaden the resulting FSSP size distribution, of which the oversized side would contribute stronger to the particle volume. To test the maximum contribution of this effect the size distribution can be reduced to one size bin of the maximum particle count. For the size distribution of maximum particle volume (11 December 2011, Fig. 15, right panel) such a maximum broadening comparison reduces the total particle volume only by 26 %. In addition, the unexpected maximum particle sizes above 20 µm in diameter are rather rare and contribute not more than 20 % to the total particle volume despite their large individual sizes. Obviously, the particle volume is very sensitive to the measured particle size and further errors due to asphericity higher than 1 : 2. Inaccurate density and refractive index assumptions might contribute as well to the size error and the overestimated particulate volume. By comparison, NAD dihydrate particles nucleated within the AIDA chamber (Wagner et al., 2005) were best explained by oblate particles with asphericities (ratio of the rotational to horizontal

ACPD
14, 12071–12120, 2014

axes) of about 1 : 5. In Woiwode et al. (2014) columnar particles with asphericities in the order of 8 : 1 and characterised by reduced settling velocities are suggested. This would result in a high degree of agreement between simulated and measured vertical redistribution of HNO_3.

4.2 Hypothesis 2: NAT-coated-ice

The second hypothesis is based on NAT layers growing on preexisting ice particles. CALIOP satellite measurements of the winter 2009/2010 show frequent ice observations (Pitts et al., 2011). For the winter 2011/2012 the temperature in the polar vortex was close to the frostpoint about one day before the measurement flight on 11 December 2011 (Fig. 2). A simple test by analyzing back trajectories (HYSPLIT[2]) results in temperatures close to the frost point over Greenland about 20 h prior to the in situ measurements. For this it was assumed that a sedimentation speed of $100\,m\,h^{-1}$ or $2.8\,cm\,s^{-1}$ corresponds to particle diameters of about 18 µm for NAT or 25 µm for ice density (Müller and Peter, 1992). It is conceivable that lee waves over Greenland resulted in even lower temperatures than resolved in the models, this way providing conditions where ice particles might have grown within minutes to significant sizes. If such particles later acquire a NAT coating with the ice evaporating when ambient temperatures rise above the frost point, then hollow NAT shells may result which have large (optical) sizes but lower HNO_3 mass than solid NAT particles of the same size. Moreover, many back trajectories (also from the RECONCILE campaign) starting from in situ measurement points lead to ambient temperatures above T_{NAT} within about 48 h prior to the measurement, which gives a pure and compact NAT particle not enough time to grow to the detected large particle diameters. A publication of Goodman et al. (1997) based on Antarctic in situ measurements shows impactor replicas of presumably ice particles of sizes of up to 30 µm, although the replicas where collected at ambient temperature of 2–3 K above the frost point. The technique used there indicated also

[2]HYSPLIT – Hybrid Single Particle Lagrangian Integrated Trajectory Model, NOAA

ACPD
14, 12071–12120, 2014

the presence of NO_3^- ions in these particles, which supports the hypothesis of a NAT layer on ice. Moreover, laboratory measurements initially conceived to prove that NAT coated ice particles can survive for some time under ambient temperatures above the frost point because of such "protective NAT coating" showed the opposite, namely, that the NAT layer does not prevent the underlying ice substrate from evaporation (Biermann et al., 1998; Peter et al., 1994). For these reasons the hypothesis of left over hollow NAT shells with large optical cross sections after the evaporation of underlying ice seems viable. Future specialized laboratory experiments should be dedicated to the exploration of this possibility.

5 Summary and conclusions

A comprehensive data set of optical in situ measurements of PSCs was obtained in two Arctic winter vortices. Cloud particles were detected on synoptic scales mostly below T_{NAT} but above ice saturation temperature. The prevailing type of detected size distribution was a mixture of the submicron sized STS and a large particle mode (around 15 µm diameter) with high HNO_3 content. The assumption of solid compact NAT particles leads to the following descrepancies: the amount of the resulting condensed HNO_3 exeeds stratospheric values, and particles settling velocities and growth times can not be reconciled with back trajectories. Maximum particle sizes derived from the NO_y-measurements are still well above the limits given by trajectory calculations. It is hypothyzed that such descrepancies can be resolved if particles are strongly aspherical or the composition of the largest particles, at least at certain stage of their formation is not pure NAT, e.g. NAT coated ice or NAT shells grown on ice. Similar to measurements of Brooks et al. (2003) and Fahey et al. (2001), the FSSP (optically) detected particle density outnumbers the density inferred from the NO_y measurements. This behavior is to be expected, if the calculation of enhancement factor of the NO_y sampling inlet did not account for large asphericity of the particles having higher aerodynamic diameters. Beyond the proposed hypotheses this work cannot clarify the precise nature of the

ACPD
14, 12071–12120, 2014

large HNO_3 containing particles. Both solutions might be possible, because it has also been shown, that NAT particles nucleate without preexisting ice particles (Voigt et al., 2003), though this publication reports particle diameters only of up to 8 µm.

Large particles introduced as "NAT rocks" seem to frequently occur in PSCs of which a substantial set of particle size distribution was collected. For the first time this particle type was detected with an optical array probe. Direct measurements of the morphology of PSC particles are highly desirable and will enable an appropriate size calibration of the FSSP for refining and possibly re-visiting the measurements presented in this work.

Acknowledgements. This work was supported by the EU under the grant number RECONCILE-226365-FP7-ENV-2008-1, and the ERC Advanced Grant No 321040 ("EX-CATRO"), as well as by the Max Planck Society. We thank our engineers Wilhelm Schneider, Christian von Glahn (MPI), Paul Stock and Michael Lichtenstern (DLR) for support of the instrument preparation and operation before and during the campaigns. The flight planning for the ESSenCe campaign was assisted by CLaMS model forecasts supported by German Research Foundation (DFG) under the project LASSO (HALO-SPP 1294/GR 3786). The teamwork of the M-55 pilots and crew, the campaign coordination team, and the other RECONCILE/ESSenCe participants and contributors is very gratefully acknowledged. We particularly thank our Russian colleagues, scientists, M-55 ground-crew, engineers, pilots and Myasishchev Design Bureau (MDB) staff for 15 years of successful and exciting collaboration on the M-55 *Geophysica* aircraft. This publication also is dedicated to the memory of our colleague – and friend –, Cornelius Schiller, who was involved in RECONCILE and ESSenCe, and who passed away on 3 March 2012.

The service charges for this open access publication have been covered by the Max Planck Society.

ACPD
14, 12071–12120, 2014

References

Baumgardner, D., Dye, J. E., Gandrud, B. W., and Knollenberg, R. G.: Interpretation of measurements made by the forward scattering spectrometer probe (FSSP-300) during the Airborne Arctic Stratospheric Expedition, J. Geophys. Res.-Atmos., 97, 8035–8046, doi:10.1029/91JD02728, 1992. 12076

Biermann, U. M., Crowley, J. N., Huthwelker, T., Moortgat, G. K., Crutzen, P. J., and Peter, T.: FTIR studies on lifetime prolongation of stratospheric ice particles due to NAT coating, Geophys. Res. Lett., 25, 3939–3942, doi:10.1029/1998GL900040, 1998. 12092

Bogdan, A., Molina, M. J., Tenhu, H., Mayer, E., and Loerting, T.: Formation of mixed-phase particles during the freezing of polar stratospheric ice clouds, Nat. Chem., 2, 197–201, doi:10.1038/nchem.540, 2010. 12075

Borrmann, S., Luo, B., and Mishchenko, M.: Application of the T-matrix method to the measurem ent of aspherical (ellipsoidal) particles with forward scattering optical particle counters, J. Aerosol Sci., 31, 789–799, doi:10.1016/S0021-8502(99)00563-7, 2000a. 12078, 12090

Borrmann, S., Thomas, A., Rudakov, V., Yushkov, V., Lepuchov, B., Deshler, T., Vinnichenko, N., Khattatov, V., and Stefanutti, L.: Stratospheric aerosol measurements in the Arctic winter of 1996/1997 with the M-55 Geophysika high-altitude research aircraft, Tellus B, 52, 1088–1103, doi:10.1034/j.1600-0889.2000.00100.x, 2000b. 12079

Brooks, S. D., Baumgardner, D., Gandrud, B., Dye, J. E., Northway, M. J., Fahey, D. W., Bui, T. P., Toon, O. B., and Tolbert, M. A.: Measurements of large stratospheric particles in the Arctic polar vortex, J. Geophys. Res., 108, 4652, doi:10.1029/2002JD003278, 2003. 12085, 12086, 12092

Cairo, F., Adriani, A., Viterbini, M., Di Donfrancesco, G., Mitev, V., Matthey, R., Bastiano, M., Redaelli, G., Dragani, R., Ferretti, R., Rizi, V., Paolucci, T., Bernardini, L., Cacciani, M., Pace, G., and Fiocco, G.: Polar stratospheric clouds observed during the Airborne Polar Experiment – Geophysica Aircraft in Antarctica (APE-GAIA) campaign, J. Geophys. Res.-Atmos., 109, D07204, doi:10.1029/2003JD003930, 2004. 12081

Carslaw, K. S., Luo, B., and Peter, T.: An analytic expression for the composition of aqueous HNO_3-H_2SO_4 stratospheric aerosols including gas phase removal of HNO_3, Geophys. Res. Lett., 22, 1877–1880, doi:10.1029/95GL01668, 1995. 12083

ACPD
14, 12071–12120, 2014

Corte, V. D., Rietmeijer, F., Rotundi, A., Ferrari, M., and Palumbo, P.: Meteoric CaO and carbon smoke particles collected in the upper stratosphere from an unanticipated source, Tellus B, 65, 20174, doi:10.3402/tellusb.v65i0.20174, 2013. 12087

Crutzen, P. J. and Arnold, F.: Nitric acid cloud formation in the cold Antarctic stratosphere: a major cause for the springtime "ozone hole", Nature, 324, 651–655, doi:10.1038/324651a0, 1986. 12074

Curtius, J., Weigel, R., Vössing, H.-J., Wernli, H., Werner, A., Volk, C.-M., Konopka, P., Krebsbach, M., Schiller, C., Roiger, A., Schlager, H., Dreiling, V., and Borrmann, S.: Observations of meteoric material and implications for aerosol nucleation in the winter Arctic lower stratosphere derived from in situ particle measurements, Atmos. Chem. Phys., 5, 3053–3069, doi:10.5194/acp-5-3053-2005, 2005. 12076

de Reus, M., Borrmann, S., Bansemer, A., Heymsfield, A. J., Weigel, R., Schiller, C., Mitev, V., Frey, W., Kunkel, D., Kürten, A., Curtius, J., Sitnikov, N. M., Ulanovsky, A., and Ravegnani, F.: Evidence for ice particles in the tropical stratosphere from in-situ measurements, Atmos. Chem. Phys., 9, 6775–6792, doi:10.5194/acp-9-6775-2009, 2009. 12080

Dörnbrack, A., Pitts, M. C., Poole, L. R., Orsolini, Y. J., Nishii, K., and Nakamura, H.: The 2009–2010 Arctic stratospheric winter – general evolution, mountain waves and predictability of an operational weather forecast model, Atmos. Chem. Phys., 12, 3659–3675, doi:10.5194/acp-12-3659-2012, 2012. 12075

Dye, J. E. and Baumgardner, D.: Evaluation of the forward scattering spectrometer probe. Part I: Electronic and optical studies, J. Atmos. Ocean. Tech., 1, 329–344, doi:10.1175/1520-0426(1984)001<0329:EOTFSS>2.0.CO;2, 1984. 12076

Dye, J. E., Baumgardner, D., Gandrud, B. W., Kawa, S. R., Kelly, K. K., Loewenstein, M., Ferry, G. V., Chan, K. R., and Gary, B. L.: Particle size distributions in Arctic polar stratospheric clouds, growth and freezing of sulfuric acid droplets, and implications for cloud formation, J. Geophys. Res.-Atmos., 97, 8015–8034, doi:10.1029/91JD02740, 1992. 12075, 12078, 12083, 12085

Ebert, M., Waigel, R., Grooß, J.-U., Kandler, K., Molleker, S., Günther, G., Vogel, B.,Weinbruch, S., and Bormannm, S.: Characterization of refractory stratospheric aerosol particles collected within the polar vortex and polar stratospheric clouds – RECONCILE/ESSENCE, in preparation, Atmos. Chem. Phys. Discuss., 2014. 12087

Engel, I., Luo, B. P., Pitts, M. C., Poole, L. R., Hoyle, C. R., Grooß, J.-U., Dörnbrack, A., and Peter, T.: Heterogeneous formation of polar stratospheric clouds – Part 2: Nucleation of ice on

ACPD
14, 12071–12120, 2014

synoptic scales, Atmos. Chem. Phys., 13, 10769–10785, doi:10.5194/acp-13-10769-2013, 2013. 12074

Fahey, D. W., Gao, R. S., Carslaw, K. S., Kettleborough, J., Popp, P. J., Northway, M. J., Holecek, J. C., Ciciora, S. C., McLaughlin, R. J., Thompson, T. L., Winkler, R. H., Baumgardner, D. G., Gandrud, B., Wennberg, P. O., Dhaniyala, S., McKinney, K., Peter, T., Salawitch, R. J., Bui, T. P., Elkins, J. W., Webster, C. R., Atlas, E. L., Jost, H., Wilson, J. C., Herman, R. L., Kleinböhl, A., and von König, M.: The detection of large HNO_3-containing particles in the winter Arctic stratosphere, Science, 291, 1026–1031, doi:10.1126/science.1057265, 2001. 12085, 12086, 12089, 12092

Frey, W., Borrmann, S., Kunkel, D., Weigel, R., de Reus, M., Schlager, H., Roiger, A., Voigt, C., Hoor, P., Curtius, J., Krämer, M., Schiller, C., Volk, C. M., Homan, C. D., Fierli, F., Di Donfrancesco, G., Ulanovsky, A., Ravegnani, F., Sitnikov, N. M., Viciani, S., D'Amato, F., Shur, G. N., Belyaev, G. V., Law, K. S., and Cairo, F.: In situ measurements of tropical cloud properties in the West African Monsoon: upper tropospheric ice clouds, Mesoscale Convective System outflow, and subvisual cirrus, Atmos. Chem. Phys., 11, 5569–5590, doi:10.5194/acp-11-5569-2011, 2011. 12080

Goodman, J., Verma, S., Pueschel, R. F., Hamill, P., Ferry, G. V., and Webster, D.: New evidence of size and composition of polar stratospheric cloud particles, Geophys. Res. Lett., 24, 615–618, doi:10.1029/97GL00256, 1997. 12091

Grooß, J.-U., Engel, I., Borrmann, S., Frey, W., Günther, G., Hoyle, C. R., Kivi, R., Luo, B. P., Molleker, S., Peter, T., Pitts, M. C., Schlager, H., Stiller, G., Vömel, H., Walker, K. A., and Müller, R.: Nitric acid trihydrate nucleation and denitrification in the Arctic stratosphere, Atmos. Chem. Phys., 14, 1055–1073, doi:10.5194/acp-14-1055-2014, 2014. 12088, 12089

Hanson, D. and Mauersberger, K.: Laboratory studies of the nitric acid trihydrate: implications for the south polar stratosphere, Geophys. Res. Lett., 15, 855–858, doi:10.1029/GL015i008p00855, 1988. 12082

Hoyle, C. R., Engel, I., Luo, B. P., Pitts, M. C., Poole, L. R., Grooß, J.-U., and Peter, T.: Heterogeneous formation of polar stratospheric clouds – Part 1: Nucleation of nitric acid trihydrate (NAT), Atmos. Chem. Phys., 13, 9577–9595, doi:10.5194/acp-13-9577-2013, 2013. 12074, 12089

Kaufmann, M., Blank, J., Friedl-Vallon, F., Gerber, D., Guggenmoser, T., Höpfner, M., Kleinert, A., Sha, M. K., Oelhaf, H., Riese, M., Suminska-Ebersoldt, O., Woiwode, W., Siddans, R., Kerridge, B., Moyna, B., Rea, S. M., and Oldfield, M.: Technical assistance for the deployment

ACPD
14, 12071–12120, 2014

of airbornelimbsounders during ESSenCe, European Space Agency, ESA-ESTEC, Technical report, available at: https://earth.esa.int/documents/10174/134665/ESSenCe_Final_Report, 2013. 12075

Kaufmann, M., Blank, J., Guggenmoser, T., Ungermann, J., Engel, A., Ern, M., Friedl-Vallon, F., Gerber, D., Grooss, J.-U., Guenther, G., Hoepfner, M., Kleinert, A., Latzko, T., Maucher, G., Neubert, T., Nordmeyer, H., Oelhaf, H., Olschewski, F., Orphal, J., Preusse, P., Schlager, H., Schneider, H., Schuettemeyer, D., Stroh, F., Suminska-Ebersoldt, O., Vogel, B., Volk, C. M., Woiwode, W., and Riese, M.: Retrieval of three-dimensional small scale structures in upper tropospheric/lower stratospheric composition as measured by GLORIA, submitted to Atmos. Meas. Tech. Discuss., 2014. 12089

Korolev, A.: Reconstruction of the sizes of spherical particles from their shadow images. Part I: Theoretical considerations, J. Atmos. Ocean. Techn., 24, 376–389, doi:10.1175/JTECH1980.1, 2007. 12076

Krieger, U. K., Mössinger, J. C., Luo, B., Weers, U., and Peter, T.: Measurement of the refractive indices of H_2SO_4-HNO_3-H_2O solutions to stratospheric temperatures, Appl. Optics, 39, 3691–3703, doi:10.1364/AO.39.003691, 2000. 12077

Lance, S., Brock, C. A., Rogers, D., and Gordon, J. A.: Water droplet calibration of the Cloud Droplet Probe (CDP) and in-flight performance in liquid, ice and mixed-phase clouds during ARCPAC, Atmos. Meas. Tech., 3, 1683–1706, doi:10.5194/amt-3-1683-2010, 2010. 12076, 12078

Larsen, N., Knudsen, B. M., Svendsen, S. H., Deshler, T., Rosen, J. M., Kivi, R., Weisser, C., Schreiner, J., Mauerberger, K., Cairo, F., Ovarlez, J., Oelhaf, H., and Spang, R.: Formation of solid particles in synoptic-scale Arctic PSCs in early winter 2002/2003, Atmos. Chem. Phys., 4, 2001–2013, doi:10.5194/acp-4-2001-2004, 2004. 12076

Lowe, D., MacKenzie, A. R., Schlager, H., Voigt, C., Dörnbrack, A., Mahoney, M. J., and Cairo, F.: Liquid particle composition and heterogeneous reactions in a mountain wave Polar Stratospheric Cloud, Atmos. Chem. Phys., 6, 3611–3623, doi:10.5194/acp-6-3611-2006, 2006. 12075

Luo, B., Krieger, U. K., and Peter, T.: Densities and refractive indices of $H_2SO_4/HNO_3/H_2O$ solutions to stratospheric temperatures, Geophys. Res. Lett., 23, 3707–3710, doi:10.1029/96GL03581, 1996. 12077

ACPD
14, 12071–12120, 2014

Marti, J. and Mauersberger, K.: A survey and new measurements of ice vapor pressure at temperatures between 170 and 250 K, Geophys. Res. Lett., 20, 363–366, doi:10.1029/93GL00105, 1993. 12082

Middlebrook, A. M., Berland, B. S., George, S. M., Tolbert, M. A., and Toon, O. B.: Real refractive indices of infrared-characterized nitric-acid/ice films: implications for optical measurements of polar stratospheric clouds, J. Geophys. Res.-Atmos., 99, 25655–25666, doi:10.1029/94JD02391, 1994. 12077

Mitev, V., Matthey, R., and Makarov, V.: Miniature backscatter lidar for cloud and aerosol observation from high altitude aircraft, Recent Res. Devel. Geophys., 4, 207–223, 2002. 12081

Mitev, V., Poole, L. R., Pitts, M. C., and Matthey, R.: Comparison case between CALIPSO Lidar and MALs on M55 Geophysica during RECONCILE Campaign, 26th International Laser Radar Conference, 25–29 July 2012, Porto Heli, Greece, 2012. 12081

Müller, R. and Peter, T.: The numerical modelling of the sedimentation of polar stratospheric cloud pariticles, Ber. Bunsen. Phys. Chem., 96, 353–361, doi:10.1002/bbpc.19920960323, 1992. 12091

Northway, M. J., Gao, R. S., Popp, P. J., Holecek, J. C., Fahey, D. W., Carslaw, K. S., Tolbert, M. A., Lait, L. R., Dhaniyala, S., Flagan, R. C., Wennberg, P. O., Mahoney, M. J., Herman, R. L., Toon, G. C., and Bui, T. P.: An analysis of large HNO_3-containing particles sampled in the Arctic stratosphere during the winter of 1999/2000, J. Geophys. Res.-Atmos., 107, SOL 41-1–SOL 41-22, doi:10.1029/2001JD001079, 2002. 12081, 12086

Peter, T.: Microphysics and heterogeneous chemistry of polar stratospheric clouds, Annu. Rev. Phys. Chem., 48, 785–822, doi:10.1146/annurev.physchem.48.1.785, 1997. 12074, 12083

Peter, T. and Grooß, J.-U.: Stratospheric Ozone Depletion and Climate Change, Chapter 4, Roy. Soc. Chem., 108–144, doi:10.1039/9781849733182, 2011. 12074

Peter, T., Müller, R., Crutzen, P. J., and Deshler, T.: The lifetime of leewave – induced ice particles in the Arctic stratosphere: II. Stabilization due to NAT-coating, Geophys. Res. Lett., 21, 1331–1334, doi:10.1029/93GL03019, 1994. 12090, 12092

Pitts, M. C., Poole, L. R., Dörnbrack, A., and Thomason, L. W.: The 2009–2010 Arctic polar stratospheric cloud season: a CALIPSO perspective, Atmos. Chem. Phys., 11, 2161–2177, doi:10.5194/acp-11-2161-2011, 2011. 12075, 12081, 12091

Shur, G., Sitnikov, N., and Drynkov, A.: A mesoscale structure of meteorological fields in the tropopause layer and in the lower stratosphere over the southern tropics (Brazil), Russ. Meteorol. Hydrol., 32, 487–494, doi:10.3103/S106837390708002X, 2007. 12082

ACPD
14, 12071–12120, 2014

Solomon, S.: Stratospheric ozone depletion: a review of concepts and history, Rev. Geophys., 37, 275–316, doi:10.1029/1999RG900008, 1999. 12074

Solomon, S., Garcia, R. R., Rowland, F. S., and Wuebbles, D. J.: On the depletion of Antarctic ozone, Nature, 321, 755–758, doi:10.1038/321755a0, 1986. 12074

Toon, O. B., Hamill, P., Turco, R. P., and Pinto, J.: Condensation of HNO_3 and HCl in the winter polar stratospheres, Geophys. Res. Lett., 13, 1284–1287, doi:10.1029/GL013i012p01284, 1986. 12074

Toon, O. B., Browell, E. V., Kinne, S., and Jordan, J.: An analysis of lidar observations of polar stratospheric clouds, Geophys. Res. Lett., 17, 393–396, doi:10.1029/GL017i004p00393, 1990. 12077

Voigt, C., Schreiner, J., Kohlmann, A., Zink, P., Mauersberger, K., Larsen, N., Deshler, T., Kroger, C., Rosen, J., Adriani, A., Cairo, F., Donfrancesco, G. D., Viterbini, M., Ovarlez, J., Ovarlez, H., David, C., and Dornbrack, A.: Nitric Acid Trihydrate (NAT) in Polar stratospheric clouds, Science, 290, 1756–1758, doi:10.1126/science.290.5497.1756, 2000. 12074

Voigt, C., Larsen, N., Deshler, T., Kröger, C., Schreiner, J., Mauersberger, K., Luo, B., Adriani, A., Cairo, F., Di Donfrancesco, G., Ovarlez, J., Ovarlez, H., Dörnbrack, A., Knudsen, B., and Rosen, J.: In situ mountain-wave polar stratospheric cloud measurements: implications for nitric acid trihydrate formation, J. Geophys. Res., 108, 8331, doi:10.1029/2001JD001185, 2003. 12075, 12093

Voigt, C., Schlager, H., Luo, B. P., Dörnbrack, A., Roiger, A., Stock, P., Curtius, J., Vössing, H., Borrmann, S., Davies, S., Konopka, P., Schiller, C., Shur, G., and Peter, T.: Nitric Acid Trihydrate (NAT) formation at low NAT supersaturation in Polar Stratospheric Clouds (PSCs), Atmos. Chem. Phys., 5, 1371–1380, doi:10.5194/acp-5-1371-2005, 2005. 12080

von Hobe, M., Bekki, S., Borrmann, S., Cairo, F., D'Amato, F., Di Donfrancesco, G., Dörnbrack, A., Ebersoldt, A., Ebert, M., Emde, C., Engel, I., Ern, M., Frey, W., Genco, S., Griessbach, S., Grooß, J.-U., Gulde, T., Günther, G., Hösen, E., Hoffmann, L., Homonnai, V., Hoyle, C. R., Isaksen, I. S. A., Jackson, D. R., Jánosi, I. M., Jones, R. L., Kandler, K., Kalicinsky, C., Keil, A., Khaykin, S. M., Khosrawi, F., Kivi, R., Kuttippurath, J., Laube, J. C., Lefèvre, F., Lehmann, R., Ludmann, S., Luo, B. P., Marchand, M., Meyer, J., Mitev, V., Molleker, S., Müller, R., Oelhaf, H., Olschewski, F., Orsolini, Y., Peter, T., Pfeilsticker, K., Piesch, C., Pitts, M. C., Poole, L. R., Pope, F. D., Ravegnani, F., Rex, M., Riese, M., Röckmann, T., Rognerud, B., Roiger, A., Rolf, C., Santee, M. L., Scheibe, M., Schiller, C., Schlager, H., Siciliani de Cumis, M., Sitnikov, N., Søvde, O. A., Spang, R., Spelten, N.,

ACPD
14, 12071–12120, 2014

Stordal, F., Sumińska-Ebersoldt, O., Ulanovski, A., Ungermann, J., Viciani, S., Volk, C. M., vom Scheidt, M., von der Gathen, P., Walker, K., Wegner, T., Weigel, R., Weinbruch, S., Wetzel, G., Wienhold, F. G., Wohltmann, I., Woiwode, W., Young, I. A. K., Yushkov, V., Zobrist, B., and Stroh, F.: Reconciliation of essential process parameters for an enhanced predictability of Arctic stratospheric ozone loss and its climate interactions (RECONCILE): activities and results, Atmos. Chem. Phys., 13, 9233–9268, doi:10.5194/acp-13-9233-2013, 2013. 12075

Wagner, R., Möhler, O., Saathoff, H., Stetzer, O., and Schurath, U.: Infrared spectrum of nitric acid dihydrate: influence of particle shape, J. Phys. Chem. A, 109, 2572–2581, doi:10.1021/jp044997u, 2005. 12074, 12090

Waibel, A. E., Peter, T., Carslaw, K. S., Oelhaf, H., Wetzel, G., Crutzen, P. J., Pöschl, U., Tsias, A., Reimer, E., and Fischer, H.: Arctic ozone loss due to denitrification, Science, 283, 2064–2069, doi:10.1126/science.283.5410.2064, 1999. 12074

Warren, J., Achilles, C., Todd, N., Bastien, R., and Zolensky, M.: Particles from Collectors L2071, L2076, L2079, L2083 and W7068, Cosmic Dust Catalog, 18, available at: http://curator.jsc.nasa.gov/dust/cdcat18 (last access: 25 April 2014), 2011. 12087

Wegner, T., Grooß, J.-U., von Hobe, M., Stroh, F., Sumińska-Ebersoldt, O., Volk, C. M., Hösen, E., Mitev, V., Shur, G., and Müller, R.: Heterogeneous chlorine activation on stratospheric aerosols and clouds in the Arctic polar vortex, Atmos. Chem. Phys., 12, 11095–11106, doi:10.5194/acp-12-11095-2012, 2012. 12074

Weigel, R., Hermann, M., Curtius, J., Voigt, C., Walter, S., Böttger, T., Lepukhov, B., Belyaev, G., and Borrmann, S.: Experimental characterization of the COndensation PArticle counting System for high altitude aircraft-borne application, Atmos. Meas. Tech., 2, 243–258, doi:10.5194/amt-2-243-2009, 2009. 12076

Weisser, C., Mauersberger, K., Schreiner, J., Larsen, N., Cairo, F., Adriani, A., Ovarlez, J., and Deshler, T.: Composition analysis of liquid particles in the Arctic stratosphere under synoptic conditions, Atmos. Chem. Phys., 6, 689–696, doi:10.5194/acp-6-689-2006, 2006. 12076

Woiwode, W., Oelhaf, H., Gulde, T., Piesch, C., Maucher, G., Ebersoldt, A., Keim, C., Höpfner, M., Khaykin, S., Ravegnani, F., Ulanovsky, A. E., Volk, C. M., Hösen, E., Dörnbrack, A., Ungermann, J., Kalicinsky, C., and Orphal, J.: MIPAS-STR measurements in the Arctic UTLS in winter/spring 2010: instrument characterization, retrieval and validation, Atmos. Meas. Tech., 5, 1205–1228, doi:10.5194/amt-5-1205-2012, 2012. 12082

Woiwode, W., Grooß, J.-U., Oelhaf, H., Molleker, S., Borrmann, S., Ebersoldt, A., Frey, W., Gulde, T., Khaykin, S., Maucher, G., Piesch, C., and Orphal, J.: Denitrification by large NAT

ACPD
14, 12071–12120, 2014

particles: the impact of reduced settling velocities and hints on particle characteristics, Atmos. Chem. Phys. Discuss., 14, 5893–5927, doi:10.5194/acpd-14-5893-2014, 2014. 12088, 12090, 12091

Worsnop, D. R., Zahniser, M. S., Fox, L. E., and Wofsy, S. C.: Vapor pressures of solid hydrates of nitric acid: implications for Polar stratospheric clouds, Science, 259, 71–74, doi:10.1126/science.259.5091.71, 1993. 12075

Zöger, M., Afchine, A., Eicke, N., Gerhards, M.-T., Klein, E., McKenna, D. S., Morschel, U., Schmidt, U., Tan, V., Tuitjer, F., Woyke, T., and Schiller, C.: Fast in situ stratospheric hygrometers: a new family of balloon-borne and airborne Lyman-alpha photofragment fluorescence hygrometers, J. Geophys. Res.-Atmos., 104, 1807–1816, doi:10.1029/1998JD100025, 1999. 12081

ACPD
14, 12071–12120, 2014

Table 1. Numbers of particles detected by the FSSP-100 compared to the number of CIPgs images detected in PSCs.

RECONCILE flight date	number of CIPgs images	FSSP-100 $D > 15\,\mu m$	FSSP-100 $D > 15\,\mu m$
20 Jan 2010	31	5*	20*
22 Jan 2010	55	16	59
24 Jan 2010	22	3	26
25 Jan 2010	149	45	111

* For flight Number 2 the data of FSSP-300 was taken and scaled to the FSSP-100's sample area.

ACPD
14, 12071–12120, 2014

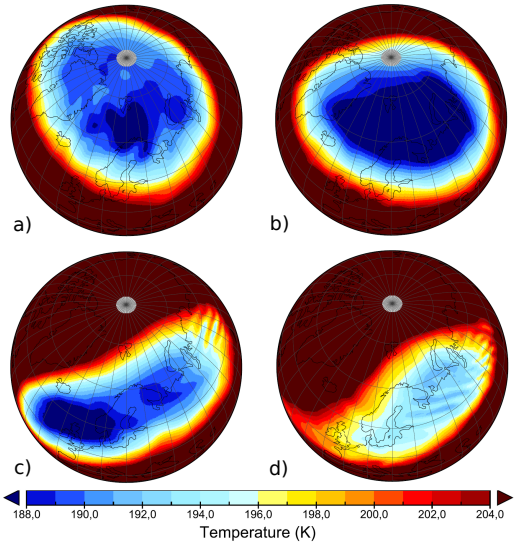

Fig. 1. ERA Interim data of temperature at 30 hPa level during RECONCILE times in January 2010: **(a)** 10 January 00:00 UTC **(b)** 17 January 12:00 UTC – corresponds to 1st PSC flight. **(c)** 25 January 12:00 UTC – last flight with PSC occurrence. **(d)** 28 January 18:00 UTC. The darkest blue color in the plot is scaled for temperature below 188 K to illustrate regions with temperatures close to, or below T_{ICE}.

ACPD
14, 12071–12120, 2014

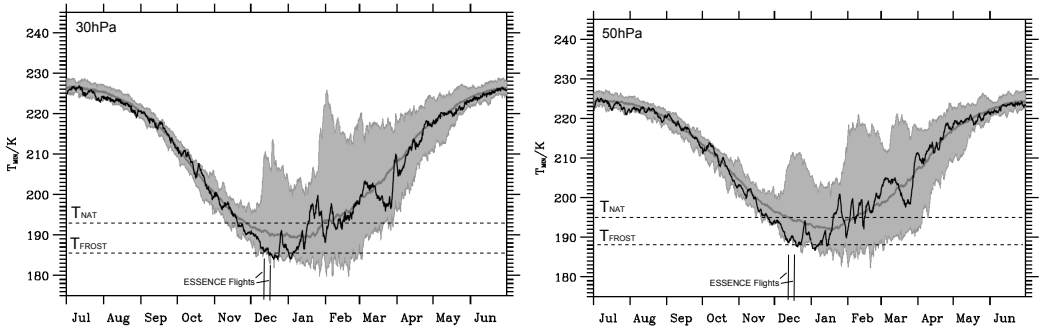

Fig. 2. Climatology of temperatures between 65° and 90° N (grey curve) and minimum temperatures (shadow area) in the region of Fig. 1 at 30 hPa (left panel) and 50 hPa (right panel) for the years between 1989 and 2009. The black curve displays the minimum temperature for the winter 2011/2012 where two flights with M-55 were conducted. The plot is an analogy to the plot provided for the winter 2009/2010 in Dörnbrack et al., 2012 with the same data source (ECMWF reanalysis at 6 hourly temporal resolutions) and PSC formation temperatures T_{NAT} and T_{ICE} calculated for 5 ppm of water vapor and 10 ppbv of nitric acid trihydrate (NAT).

ACPD
14, 12071–12120, 2014

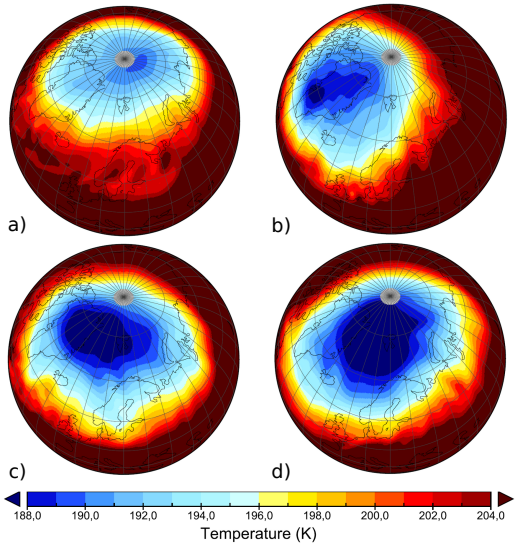

Fig. 3. ERA Interim Data of temperature at 30 hPa level during the ESSenCe campaign on the following times in December 2011: **(a)** 4 December 00:00 UTC, **(b)** 8 December 18:00 UTC, **(c)** 11 December 12:00 UTC – corresponding to the first flight, **(d)** 16 December 18:00 UTC – close to the second flight. The polar vortex established during December 2011.

ACPD
14, 12071–12120, 2014

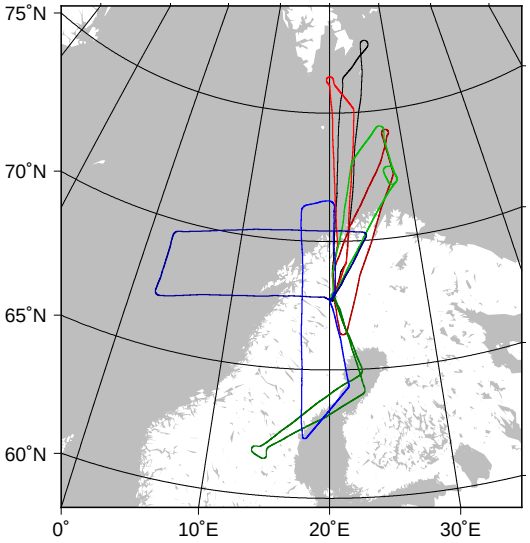

Fig. 4. Flight tracks of five PSC-Flights from the RECONCILE-Campaign performed in January 2010 are shown with two additional flights performed in December 2011 (ESSenCe-Campaign). All flights were performed out of Kiruna, Sweden. RECONCILE-Flights numbers 1 to 5 are marked: black (17 January), red (20 January), dark red (22 January), green (24 January), dark green (25 January 2010). ESSenCe flights: blue (11 December 2011) and dark blue (16 December 2011).

ACPD
14, 12071–12120, 2014

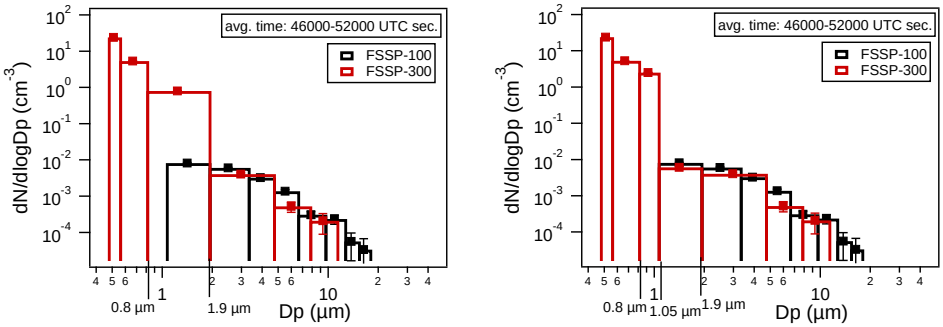

Fig. 5. Size distributions of the FSSP-100 and FSSP-300 from a PSC encounter of 1.67 h duration are compared for the complete PSC-event during the first RECONCILE-flight (17 January 2010). The sizing of particles between about 0.8 and 1.9 µm is uncertain due to ambiguity in the Mie-calibration curve. This is taken into account by the wide size bin, which consists of several instrumental raw size bins. At the same time the detected particle numbers exhibit a decrease of about two orders of magnitude over this size range. Assuming that most of the particles belong to the STS-Mode with spherical shape and sizes closer to the lower bin limit, the discrepancy of the FSSP-100 and FSSP-300 can be explained. This is shown in the right panel, where the FSSP-300 size bin is divided by ignoring the ambiguity inherent in the Mie-curve. The initially "suspected" apparent discrepancy between the two instruments in the overlapping bin can be understood this way.

ACPD
14, 12071–12120, 2014

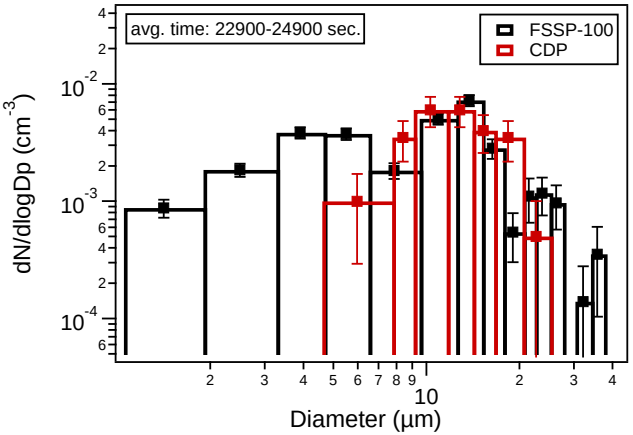

Fig. 6. Size distribution of the FSSP-100 and CDP measured on the flight on 25 January 2010. Due to instrumental problems only in this one flight of the RECONCILE-campaign the particles detection of the CDP worked well with a higher than usual detection size limit of about 5–8 µm. At the same time the largest PSC-particles in relatively high numbers were present in this flight. Note though that the FSSP-size bins above 30 µm contain only 3 counts.

ACPD
14, 12071–12120, 2014

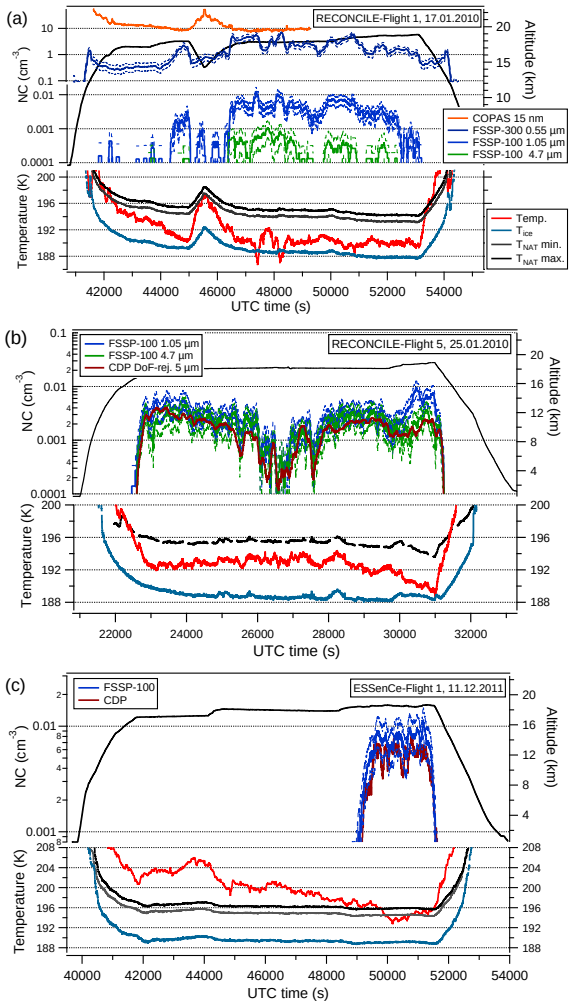

ACPD
14, 12071–12120, 2014

In situ measurements of large HNO_3 containing particles in the Arctic vortex

S. Molleker et al.

Fig. 7. Time series of the FSSP measurements of two RECONCILE and one ESSenCe flights overlaid with relevant temperatures: ambient temperature (red), NAT equilibrium T_{NAT} (black, grey) and frostpoint T_{ICE} (blue). T_{NAT} is estimated for 5 and 10 ppbv of HNO_3 if no in situ NO_y data is available; otherwise in situ SIOUX-NO_y data was used. **(a)** For the flight of 17 January 2010 FSSP-300-data is available and is compared to the particle number concentration measured by COPAS, with a detection limit of 15 nm. **(b)** RECONCILE-Flight on 25 January 2010. In this flight, the highest density of large (20–30 µm) HNO_3-containing particles of the campaign was encountered. Despite detection problems on the CDP for the smallest particles, the detection and counting of the DoF-rejected particles (dark red curve) worked well showing very good agreement to the FSSP-100 curve for 4.7 µm cutoff (green). Note that the curve deduced from the DoF-rejected events has much better counting statistics. **(c)** ESSenCe-flight on 11 December 2011 with simultaneous measurement of the CDP and FSSP-100. Here the synoptic scale of PSCs is apparent between 46 000 and 53 000 UT seconds (upper panel). Upper and low dashed lines indicate the uncertainty due to the uncertainty of sample volume and counting statistics.

ACPD
14, 12071–12120, 2014

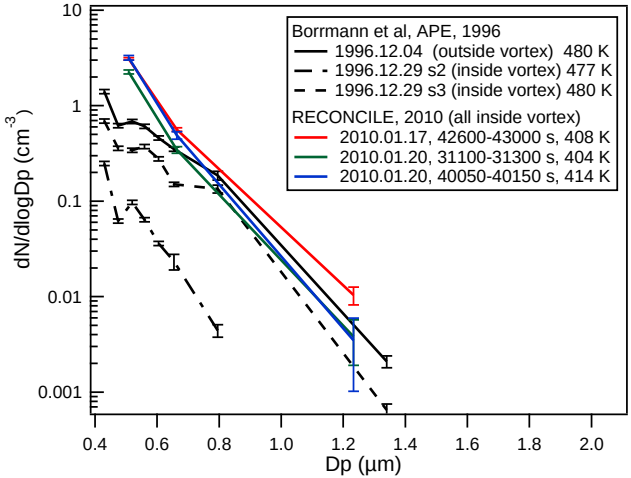

Fig. 8. FSSP-300 size distributions of background aerosol from comparable meteorological situations. Here only measurements outside of PSCs are compared with old measurements during the APE-Campaign (1996) of the same instrument (Borrmann et al., 2000a), whereby the instrument was upgraded with a new electronics module (SPP-300 from DMT, Boulder, Co, USA; among other modifications) in between. Here this data is merely considered for instrument intercomparison and compatibility purposes, as the measurements show a consistent picture. Note however, the size distribution denoted as "s2" is deep inside the vortex where 1996 record low particle number densities were found. Disregarding "s2" the background number concentrations are very similar considering also the different polar vortices.

ACPD
14, 12071–12120, 2014

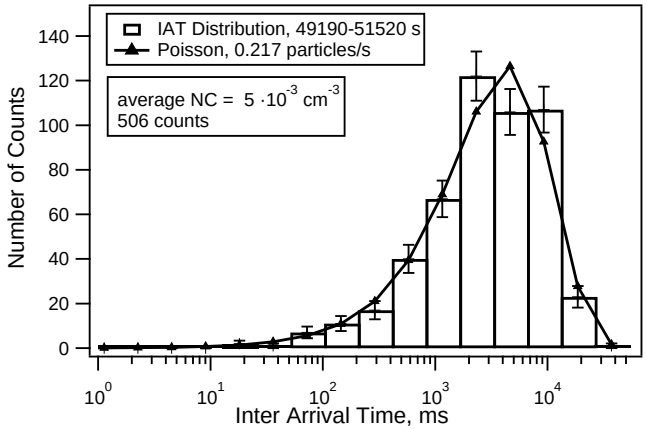

Fig. 9. Distribution of the inter arrival times (IAT) based on the CDP's particle by particle data is used to check the quality of the PSC-measurement (11 December 2011). The distribution shows inter arrival times of PSC-particles detected in about 40 min of flight time (i.e. 400 km) which is in a good agreement with the Poisson statistics (triangle marks). This implies that the detected particles were randomly distributed in a homogeneous cloud field. The CDP's (or FSSP's) counting statistics are not sufficient to resolve small spatial variations in the number density on a scale below about 200–400 km.

ACPD
14, 12071–12120, 2014

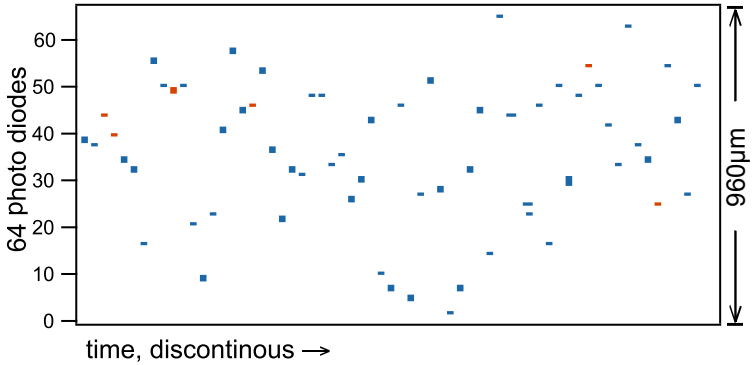

Fig. 10. Example of the 62 CIP grey scale images recorded over about 30 min during a flight on 25 January 2010 in the PSC field where FSSP-100 detected numbers of particles larger than 10 µm. Most of the pixels where triggered by the first shadow threshold at 35 % (blue color). The second threshold at 50 % (red) accounts only for less than a tenth of detected events. About 150 images were detected in this flight and 108 more images in three further PSC-flights. These image-blotches can be considered as visual proof for the existence of NAT-rock sized PSC particles.

ACPD
14, 12071–12120, 2014

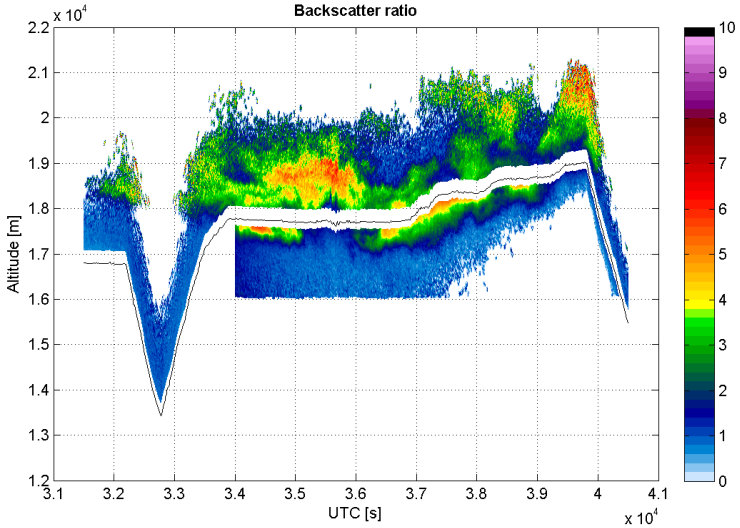

Fig. 11. Backscatter ratio profile of two lidars (MAL1 and MAL2) operated onboard the aircraft for the second part of the flight on 20 January 2010. A PSC field is visible along a flight leg of about 900 km length. Due to limitations in the dynamical range of the lidars, data from a distance less than 200 m to the aircraft is not recorded.

ACPD
14, 12071–12120, 2014

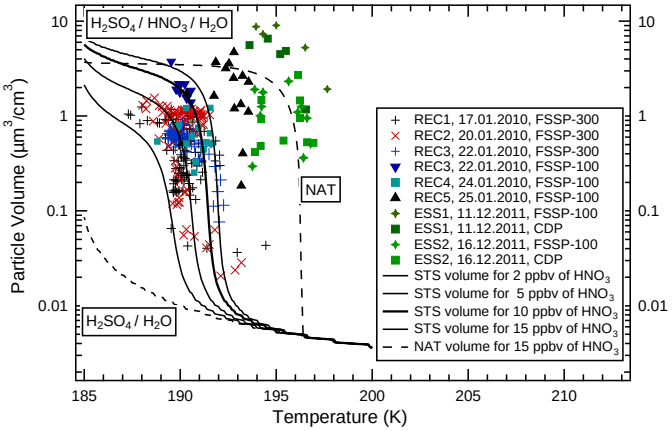

Fig. 12. Measured particle volumes vs. temperature and theoretical calculations as discussed in Peter et al., 1997. The STS-mode size range was partly resolved by the FSSP-300. The measured data points are designated as crosses, which also indicate that only particle diameters below 2 µm were integrated for calculation of the particle volume. The theoretical curve for STS volume was calculated according to Carslaw et al., 1995 with the FSSP-300 lower cut off at 0.46 µm. Four curves for different mixing ratios of HNO_3 of 2, 5, 10 and 15 ppbv are plotted. Filled symbols contain only volumes including particle diameters above 2 µm. The dashed lines for binary and ternary solutions are adopted from Peter et al., 1997 (which assumed a FSSP-300 lower size detection limit of 0.3 µm).

ACPD
14, 12071–12120, 2014

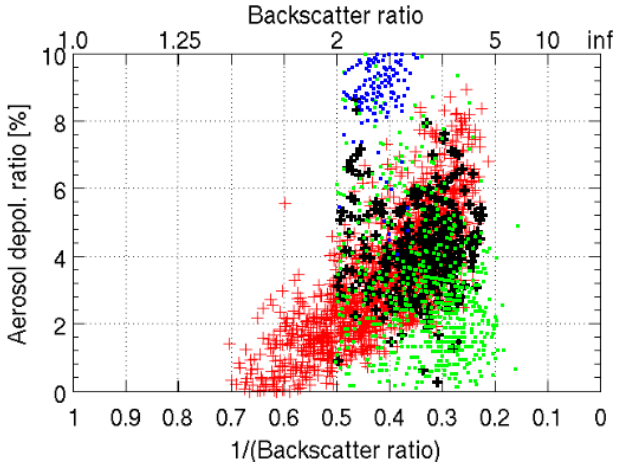

Fig. 13. Scatterplot of aerosol depolarization vs. backscatter ratio as measured by the lidar MAL (red crosses) on 20 January (see Fig. 11), and near in situ by the backscattersonde MAS, on 17 January (green squares), 20 January (black crosses), 25 January (blue squares).

ACPD
14, 12071–12120, 2014

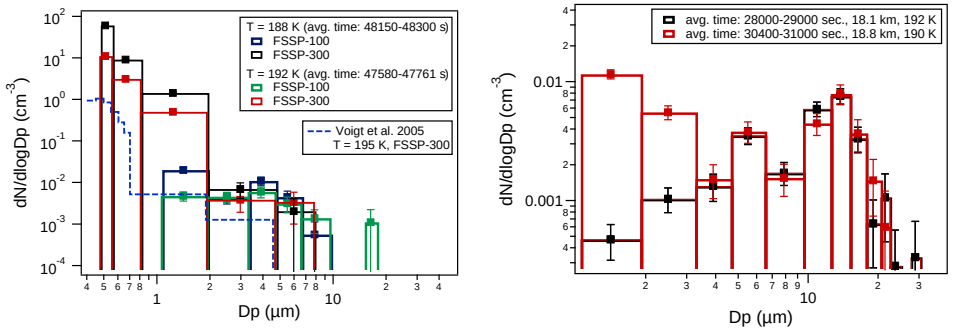

Fig. 14. Size distributions of synoptic scale Arctic PSCs as taken from successive time intervals within same flight (left panel: 17 January 2010 and right panel: 25 January 2010) but with different temperatures and altitudes. On the left panel, for comparison a FSSP-300 size distribution from a lee wave PSC (Voigt et al., 2005) is integrated, where atmospheric conditions of heterogeneous NAT nucleation without the preexistence of ice particles were encountered. The counting statistics is such that no error bars are visible in the graph for the smallest particles. These two figures show the NAT rock mode and the STS mode as distinguishably separate modes. On the right panel the NAT size range may contain an additional, separate particle mode at about 5 to 6 µm.

ACPD
14, 12071–12120, 2014

In situ measurements of large HNO_3 containing particles in the Arctic vortex

S. Molleker et al.

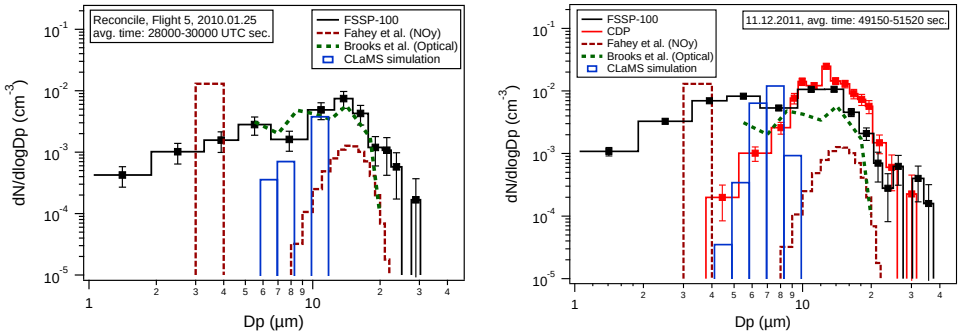

Fig. 15. Size distributions of large HNO_3-contaning PSC particles with the highest number densities from the 2010 and 2011 campaigns. RECONCILE-flight on 25 January 2010 (left panel). ESSenCe-flight on 11 December 2011 (right panel) where the number density and particle volume is about a factor of 2 higher compared with the largest values from RECONCILE. CLaMS model simulations (blue) for the corresponding coordinates of space and time do not reproduce NAT particle diameters above 12 µm. Both measurements are compared to similar findings in Fahey et al., 2001 (retrieved from total NO_y) and Brooks et al., 2003 (optical measurements).

ACPD
14, 12071–12120, 2014

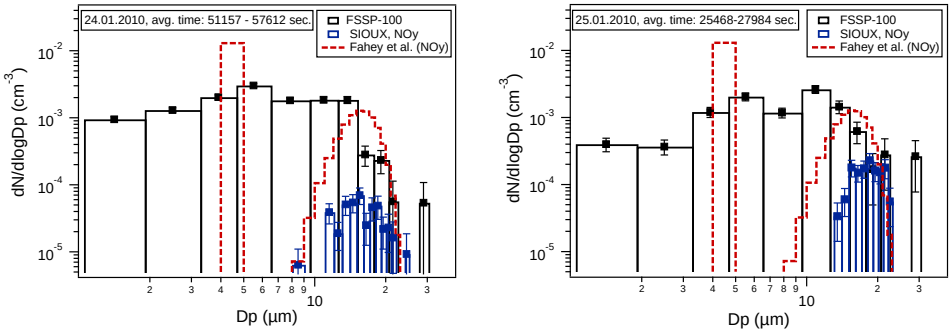

Fig. 16. Size distributions of the FSSP-100 data for time intervals where the total NO_y data of the SIOUX instruments allowed extraction of particle date from single peaks, and for which diameters assuming NAT composition were derived. The sensitivity of the NO_y instrument scales with particle volume, so that sizes only above about 10 µm could be extracted. A particle size independent enhancement factor was used, which might explain some of the discrepancy in the particle numbers between the NO_y and the optical measurements.

ACPD
14, 12071–12120, 2014

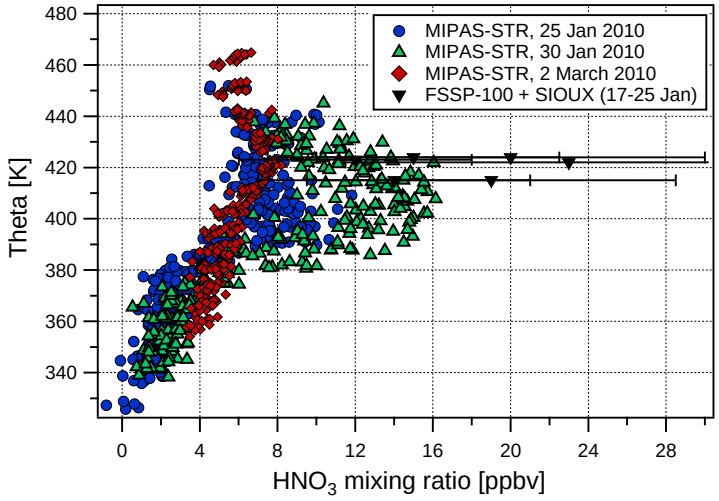

Fig. 17. Gas-phase HNO_3 mixing ratios retrieved from MIPAS-STR observations (also operated on board the M-55 Geophysica) vs. potential temperature. Enhanced HNO_3 mixing ratios are observed between 380 and 440 K as a result of renitrification. The most prominent renitrification signal is found for 30 January 2010 (green) (i.e. just after the PSC season as evident from Fig. 2) with about 9 ppbv excess HNO_3 due to renitrification. Total HNO_3 mixing ratios (condensed plus gas-phase) derived from the FSSP-100 measurements together with measured SIOUX in situ gas-phase HNO_3 partly lie within the range of MIPAS-STR and partly exceed these values. (In the case of no available SIOUX data lower and upper limits of 2 to 7 ppbv were used.) The error bars for the FSSP+SIOUX derived mixing ratios are estimated at 50 %.

ACPD
14, 12071–12120, 2014